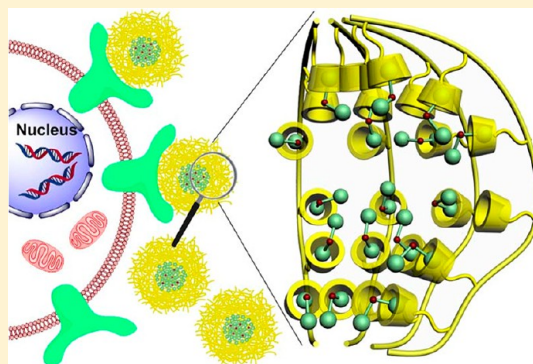


Targeted Polysaccharide Nanoparticle for Adamplatin Prodrug Delivery

Yang Yang,[†] Ying-Ming Zhang,[†] Yong Chen,[†] Jia-Tong Chen,[‡] and Yu Liu^{*†}[†]Department of Chemistry, State Key Laboratory of Elemento-Organic Chemistry, Collaborative Innovation Center of Chemical Science and Engineering and [‡]Department of Biochemistry and Molecular Biology, College of Life Sciences, Nankai University, Tianjin 300071, P. R. China

S Supporting Information

ABSTRACT: A series of conjugated hyaluronic acid particles (HAP), composed of a hydrophobic anticancer drug core and hydrophilic cyclodextrin/hyaluronic acid shell, were prepared through self-assembling and characterized by ¹H NMR titration, electron microscopy, zeta potential, and dynamic light-scattering experiments. The nanometer-sized HAP thus prepared was biocompatible and biodegradable and was well-recognized by the hyaluronic acid receptors overexpressed on the surface of cancer cells, which enabled us to exploit HAP as an efficient targeted delivery system for anticancer drugs. Indeed, HAP exhibited anticancer activities comparable to the commercial anticancer drug cisplatin but with lower side effects both in vitro and in vivo.



■ INTRODUCTION

The design of advanced drug-delivery systems with high therapeutic efficacy toward malignant tumors and insignificant toxicity to normal tissues is still one of the most challenging tasks in medicinal chemistry.¹ For an effective drug-delivery system, a high level of water solubility, controlled release, targeted delivery, biocompatibility and biodegradability, and simplified delivery should all be incorporated. In recent years, a variety of supramolecular drug-delivery systems, including liposomes,^{2–4} inorganic nanoparticles,^{5–8} polymeric micelles,^{9–13} and carbon nanomaterials,^{14–19} have been constructed from multiple functional components through non-covalent interactions. However, some concerns still remain for these delivery systems regarding the potential for long-term toxicity as well as the metabolic fate.^{20–22} Consequently, the clever design and prudent choice of materials are vital to the development of new advanced drug-delivery systems.

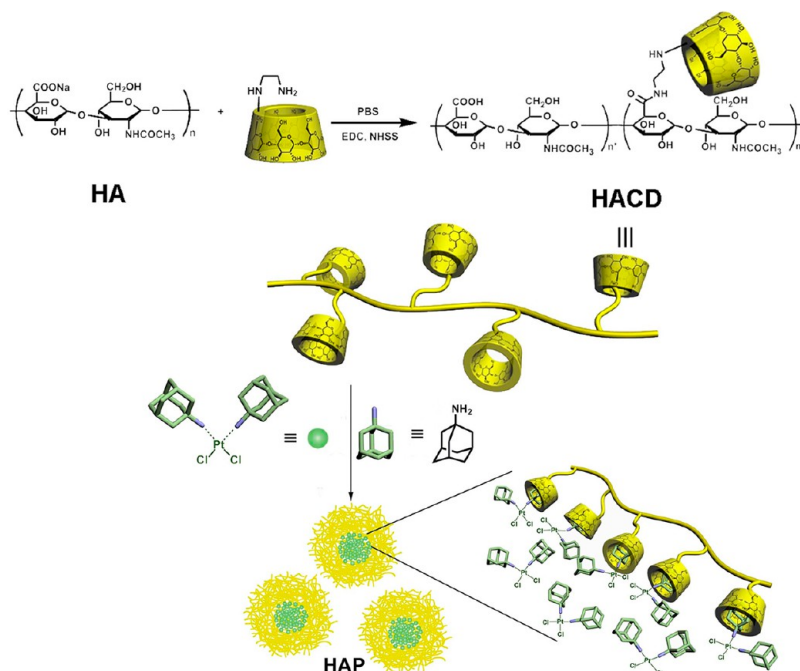
Polysaccharides have been widely exploited as building blocks for constructing nanometer-sized particles for drug delivery because of their excellent properties such as low toxicity, biocompatibility, biodegradability, stability, low cost, hydrophilicity, bioadhesion ability, and facile chemical modification.^{23–27} In particular, hyaluronic acid (HA), a water-soluble biocompatible and biodegradable polysaccharide, has been used as a targeting agent and delivery vehicle in many drug-delivery systems and also as a diagnostic agent for carcinoma^{28–30} because it can specifically recognize various cancer cells that overexpress HA receptors (CD44 and RHAMM (hyaluronan-mediated motility receptor)) on the cell surface.^{31–36} For instance, Kim, Park, and co-workers^{37–40} reported that nanoparticles composed of 5 β -cholanolic acid and

near-infrared fluorescence dye bound to HA recognized malignant tumor cells and tissues in vitro and in vivo. Peer, Shimaoka, and co-workers^{41,42} constructed liposome-based nanoparticles covered with HA, encapsulating condensed small-interfering RNA, that selectively targeted leukocyte integrins to achieve highly efficient intracellular delivery and gene-silencing activities in vivo. Lee, Chen, and co-workers⁴³ demonstrated that Zn^{II}-dipicolylamine complexes tethered to HA strongly bound siRNA and delivered it into HA-receptor-positive cancer cells.

In the present work, we chose cyclodextrin (CD) as a polysaccharide to be grafted to the HA backbone because CD is water-soluble, nontoxic, and commercially available at low cost and because, more importantly, CD can host various inorganic/organic/bioorganic molecules and ions in its hydrophobic cavity with high size/shape selectivity both in aqueous solution and solid state. Additionally, CDs have been used as convenient building blocks for constructing nanostructured functional and bioactive materials.^{44,45} As a consequence of the encapsulation of the hydrophobic moiety of drug into the CD cavity, anticancer drugs and prodrugs, such as adamplatin, are noncovalently bound to the conjugated polysaccharide, which eventually self-assemble to form nanoparticles (HAP, Scheme 1). The use of HAP as a targeted drug-delivery system is inherently advantageous because of three attributes: (1) HAP has a hydrophilic HA backbone that specifically recognizes cancer cells and concomitantly protects adamplatin prodrug from the aqueous environment that inactivates cisplatin⁴⁶

Received: September 12, 2013

Published: November 19, 2013

Scheme 1. Chemical Structures and Synthetic Routes for HACD and HAP^a

^aHACDs were synthesized by side-chain modification using an amide condensation reaction.

Table 1. Characterization of HACDs with Different Degrees of Substitution

sample	feed ratio ^a	M_w ^b	M_w ^c	M_n ^d	M_w/M_n	DS	R_h (nm) ^e
HA	0	4.6×10^4 ^f	4.8×10^4	3.1×10^4	1.54	none	10.4
HACD-5.6	0.25	5.0×10^4	5.5×10^4	3.3×10^4	1.66	5.58	10.4
HACD-11.5	0.5	5.7×10^4	5.8×10^4	3.6×10^4	1.60	11.50	10.4
HACD-16	1	6.3×10^4	6.7×10^4	4.0×10^4	1.68	16.43	10.4
HACD-17	2	6.4×10^4	6.9×10^4	4.1×10^4	1.69	17.16	10.3

^aMolar feed ratio of β -cyclodextrin to sugar residues of HA polymer. ^bMolecular weights were estimated from ¹H NMR spectra. ^cWeight-averaged molecular weights were obtained from GPC. ^dNumber-averaged molecular weights were obtained from GPC. ^eHydrodynamic radius of HACDs were measured by a viscosity detector in GPC experiment in PBS. ^fMolecular weights were obtained according to the specification of sodium hyaluronate purchased from commercial sources.

before it can reach the malignant tissues, (2) numerous CDs incorporated in HAP efficiently carry adamaptin prodrugs through encapsulation of the adamantyl group,⁴⁷ and (3) after entering a cancer cell through receptor-mediated endocytosis, encapsulated adamaptin prodrug is released through the enzyme-triggered degradation of HAP by HA-degrading intracellular enzymes, hyaluronidase-1 and -2 (Hyal-1 and -2), that are overexpressed in tumor tissues.^{43,48–51} This strategy is expected to provide a simple and versatile approach to the design and fabrication of various supramolecular targeted drug-delivery systems with high activity and low toxicity.

RESULTS AND DISCUSSION

Synthesis. A series of HACDs, incorporating 5.6–17 β -CDs grafted to a HA chain, were synthesized by the amide condensation reaction of sodium hyaluronate with mono-6-deoxy-6-ethylenediamino- β -CD in phosphate buffer solution (PBS) and characterized by ¹H NMR spectroscopy and gel permeation chromatography (GPC). The number of grafted β -CDs per HA, here defined as the degree of substitution (DS), was controlled by changing the feed ratio of mono-6-deoxy-6-ethylenediamino- β -CD to HA polymer. As can be seen from Figure S1, ¹H NMR spectra of HACDs showed the

characteristic signal of H1 proton of β -CD at ca. 5 ppm and signals assignable to HA protons and β -CD's H2–H6 protons at 3 to 4 ppm. The DS was determined by comparing the integrated peak area of the H1 proton of β -CD versus that of the *N*-acetyl protons of HA at 1.97 ppm. In view of the fact that at least six repeating units of HA are needed for achieving multiple HA–CD44 interactions in the tumor-targeting bioconjugates bearing HA and cytotoxic agents,⁵² the HACDs obtained in the present study are considered to have enough numbers of repeating units to interact with CD44. Moreover, the weight-averaged molecular weights (M_w) of HACDs determined by GPC (M_w values were determined by SEC columns with reference to poly(ethylene oxide), see Figures S2–S6, Supporting Information) matched well with the molecular weights evaluated from ¹H NMR spectra, and the DS and molecular weight of HACD decreased as the feed ratio of β -CD was reduced. The characterization data for HACDs of different DSs are summarized in Table 1. Adamaptin prodrug was synthesized by a reported method⁵³ with slight modification. It is known that the modification of cisplatin with adamantane does not impede its anticancer activity.⁵⁴ By using a modified thiourea reaction,⁵⁵ the configuration of

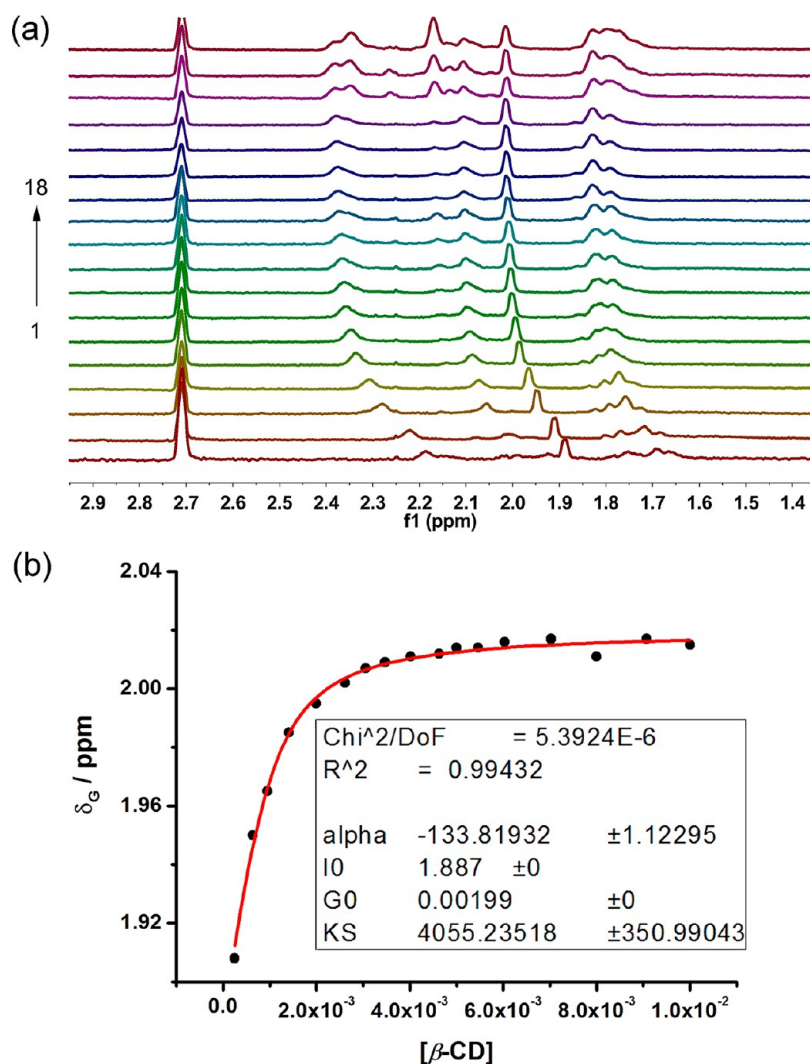


Figure 1. ¹H NMR spectral titration of adamplatin prodrug with native β -CD. (a) ¹H NMR spectra of 1 mM adamplatin upon addition of 0, 0.2, 0.6, 1.0, 1.4, 2.0, 2.6, 3.0, 3.4, 4.0, 4.6, 5.0, 5.4, 6.0, 7.0, 8.0, 9.0, and 10.0 mM β -CD (spectrum 1–18) in D₂O containing 5% DMSO-*d*₆ at 25 °C. (b) Nonlinear least-squares fit of the chemical-shift changes of the adamantyl proton peak at δ 1.9 (panel a) as a function of the β -CD concentration.

adamplatin prodrug was confirmed to be the *cis* isomer (see Figures S7 and S8, Supporting Information).

Complexation of Adamplatin Prodrug with β -CD. We employed native β -CD as a reference host to evaluate the complexation behavior of adamplatin prodrug with the β -CDs tethered to HA. As shown in Figure 1a, the ¹H NMR signals of adamantyl protons showed gradual downfield shifts with accompanying shape changes upon incremental addition of β -CD, indicating inclusion of the adamantyl moiety of adamplatin prodrug in the β -CD cavity.⁵⁶ In addition, the Job's plot showed a maximum at a molar fraction of 0.5 (see Figure S9, Supporting Information), indicating a 1:1 stoichiometry between the adamplatin prodrug and β -CD. This is reasonable because the two *cis*-adamantyls of adamplatin cannot be simultaneously accommodated in two β -CD cavities as a result of the large steric hindrance. A nonlinear least-squares fit of the titration data (Figure 1b) allowed us to determine the stability constant (K_S) of adamplatin prodrug with β -CD as $(4.1 \pm 0.4) \times 10^3 \text{ M}^{-1}$. Similarly, the adamantyl protons of adamplatin showed downfield shifts upon addition of HACD-17, but they were unchanged upon addition of sodium hyaluronate (see Figure S10, Supporting Information). These results support the

formation of a HACD/adamplatin assembly through the noncovalent interactions of multiple adamplatin molecules with the β -CD moieties of HACD.

Characterization of HAP. The facile binding of adamplatin by the β -CD units in HACD enabled us to prepare HAP by simply mixing HACD and adamplatin. High-resolution transmission electron microscopy (HR-TEM), atomic force microscopy (AFM), scanning electron microscopy (SEM), dynamic light scattering (DLS), and zeta potential experiments revealed the morphological and structural features of HAPs. The HR-TEM images shown in Figures 2a and S11 indicate that HAP-17, HAP-16, HAP-11.5, and HAP-5.6 exist as spherical nanoparticles with average diameters of ca. 60, 70, 90, and 150 nm, respectively, and that these particles tend to aggregate during the preparation process through hydrogen-bonding interactions of carboxylic and hydroxyl groups in HACDs. A series of HAP-17 nanoparticles, containing the β -CD unit and adamplatin prodrug at different ratios, were prepared to elucidate the relationship between the DS and the HAP size. TEM images revealed that the diameter of HAP-17 dramatically increased from 70 to 380 nm with decreasing adamplatin content (see Figure S12, Supporting Information).

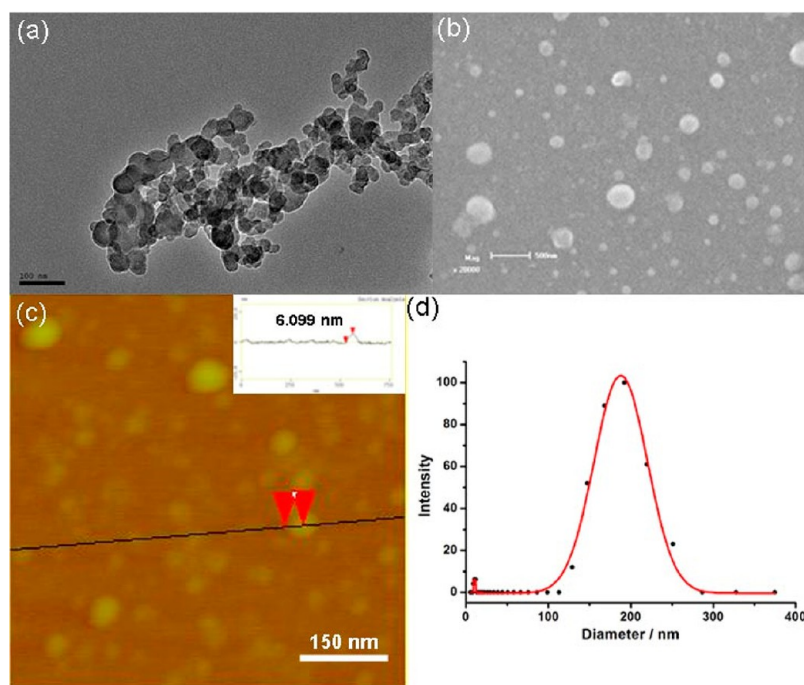


Figure 2. Typical (a) TEM, (b) SEM, and (c) AFM images of HAP-17. (d) DLS result for CONTIN plots of HAP-17 in PBS.

This result suggests that the hydrophobicity of adamplatin prodrug included in the cavity of β -CD plays an important role in determining the particle size. Thus, the low DS and therefore low drug loading in HACD-5.6 led to the formation of less compact hydrophobic cores and larger-sized aggregates among the polysaccharide nanoparticles prepared.

The SEM image (Figure 2b) gave similar morphological information, showing many aggregated nanoparticles. The AFM and SEM images of control samples (see Figures S13 and S14, Supporting Information) showed amorphous structures for sodium hyaluronate and HACD. The AFM image also revealed the fine structure and dimension of HAP-17. As shown in Figure 2c, the height of a collapsed nanoparticle was ca. 6.1 nm, which is very close to the total height of two β -CD cavities (ca. 1.7 nm), two included adamplatin (ca. 2.0 nm), and two saccharide units of hyaluronic acid (1.8 nm). The DLS results showed that HAP aggregates have a narrow distribution with a hydrodynamic diameter of ca. 180 nm calculated by cumulant analysis (Figure 2d).

Furthermore, the zeta potential of HAP was measured as ca. -20 mV (see Figure S15, Supporting Information), and this negatively charged biocompatible surface of HAP may prolong the circulation time of HAP in vivo,³⁷ eventually facilitating the delivery and release of adamplatin prodrug. Additionally, the formation of HAP was also readily apparent by visible observation (see Figure S16, Supporting Information). GPC analyses revealed that the hydrodynamic radii (R_h) of HACDs with different DSs were nearly the same at ca. 10 nm, and the aqueous solution of HACDs showed a weak Tyndall effect.⁵⁷ Upon complexation of adamplatin, the Tyndall effect was observed with great enhancement, indicative of the formation of larger aggregates in solution.

The biocompatibilities of adamplatin prodrug itself and HAP-17 were comparatively studied in PBS. Adamplatin prodrug was dispersible in water by adding DMSO as cosolvent, but it immediately precipitated in PBS at 2 mM concentration even in the presence of DMSO (see Figure S17B,

Supporting Information). In contrast, as a consequence of the hydrophilic hyaluronic acid shells incorporated, HAP-17 was well-dispersed in PBS for months even at a net adamplatin prodrug concentration of 2 mM (see Figure S17A, Supporting Information). In addition, we further performed DLS and zeta potential experiments of HAP-17 in a 10% fetal calf serum (FCS) solution. As seen in Figure S18, FCS alone exhibited two main diameter distributions around 8 and 50 nm, and the mean hydrodynamic diameter was calculated as 23.5 nm. After adding HAP-17, three diameter distributions were shown in the DLS data; that is, the ones around 7 and 40 nm were assigned to FCS, and the one around 160 nm was assigned to HAP-17. The mean hydrodynamic diameter was calculated as 96 nm, corresponding to the average diameter values of FCS and HAP-17. Similarly, the zeta potential of HAP-17 in FCS (-13 mV) was also ascribable to the joint contribution of FCS (-6.3 mV) and HAP-17 (-20 mV). Collectively, these results may demonstrate that the serum environment cannot dramatically affect the stability of HAP-17 in vitro and in vivo. The enhanced biocompatibility could facilitate the accumulation of HAP-17 nanoparticles specifically in tumor tissue sites, as described later. The loading level of adamplatin in HAP-17 was studied by atomic emission spectrometry. As shown in Figure 3a, the Pt content maximized at a 1:1 adamplatin prodrug/ β -CD ratio, and no flocculation was observed in the presence of excess HACD-17 (Figure 3b), implying a near optimal condition for preparing polysaccharide nanoparticles. Consequently, the polysaccharide nanoparticles comprising equimolar adamplatin prodrug and β -CD units were subjected to further cytotoxicity and tumor-growth inhibition studies.

The biodegradation and releasing behavior of HAP in vitro were investigated by performing the enzymatic hydrolysis of HA. As shown in Figure 4, although the hydrodynamic diameter of HAP-17 was maintained at ca. 150 nm, the scattered-light intensity dramatically decreased by approximately 90% in the presence of hyaluronidase. Moreover, no spherical structure of HAP-17 was observed in the TEM image,

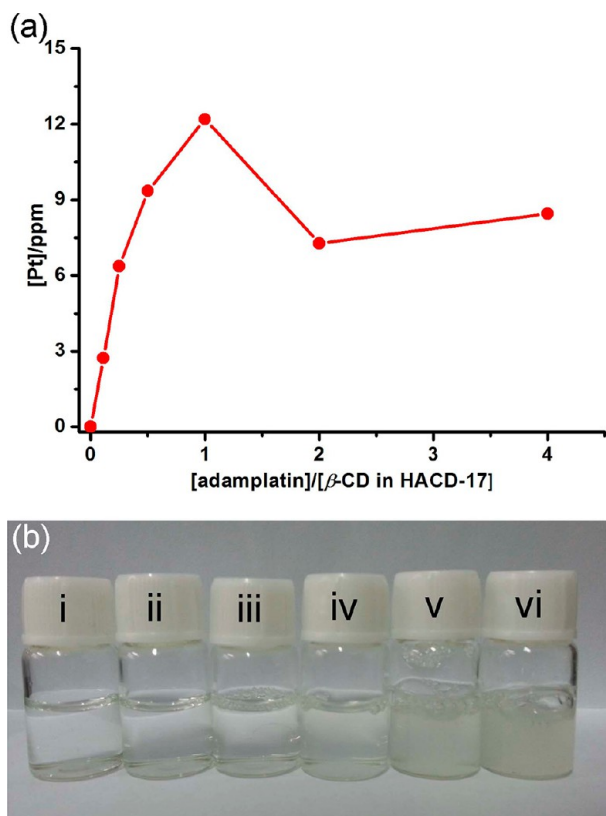


Figure 3. (a) [Pt] in HAP-17 as a function of the adamplatin/ β -CD in HACD-17 ratio. (b) Photographs of HAP-17 solutions after injecting adamplatin of 0.057, 0.13, 0.26, 0.52, 1.03, and 2.06 mM concentrations (i–vi) into HACD-17 ($[\beta$ -CD in HACD-17] = 0.51 mM).

in nice agreement with the disappearance of the Tyndall effect after the treatment with hyaluronidase. These results jointly indicated that the obtained polysaccharide nanoparticles were disassembled as soon as the endo-*N*-acetylhexosaminic bonds in the hyaluronic acid chains were specifically hydrolyzed to low-molecular-weight oligomers upon exposure to hyaluronidase.⁵⁸

Anticancer Activities in Vitro. Cytotoxicity experiments were performed to evaluate the anticancer activities of HAP in vitro, where HAP-17 was used as a candidate nanoparticle for the anticancer treatment because of its small size, facilitating the receptor-mediated endocytosis of cancer cells. As shown in Figure S19, the IC_{50} values of cisplatin, adamplatin, and HAP-17 toward the MCF-7 cell line (a type of human breast cancer cells that abundantly overexpress HA receptors on the cell surface^{33,59}) were measured as 27,⁶⁰ 8.2, and 5.6 μ M, respectively, by the MTT assay, which indicated the enhanced anticancer activity of HAP-17. In addition, as shown in Figure 5a, HAP-17 displayed a better anticancer activity than cisplatin, adamplatin prodrug, and adamplatin/ β -cyclodextrin complex toward MCF-7 cancer cells. Compared with cisplatin, which also enters MCF-7 cancer cells by membrane permeation, lipophilic adamplatin prodrug more effectively penetrates into the lipid bilayer of the cell membrane and shows better anticancer activity. By lacking the specific HA components, the nontargeted adamplatin/ β -CD complex exhibited a relatively high cytotoxicity toward both normal and cancer cells. The hydrophilic HA shell of HAP-17 specifically recognizes MCF-7 cancer cells by strongly binding to HA receptors on the cell surface, and it enters cells through receptor-mediated endocytosis. Subsequently, the nanoparticle disassembles to release the adamplatin moiety. As a result, HAP-17 shows the best anticancer activities toward MCF-7 cancer cell lines. Moreover, the anticancer activity of HAP-17 dramatically

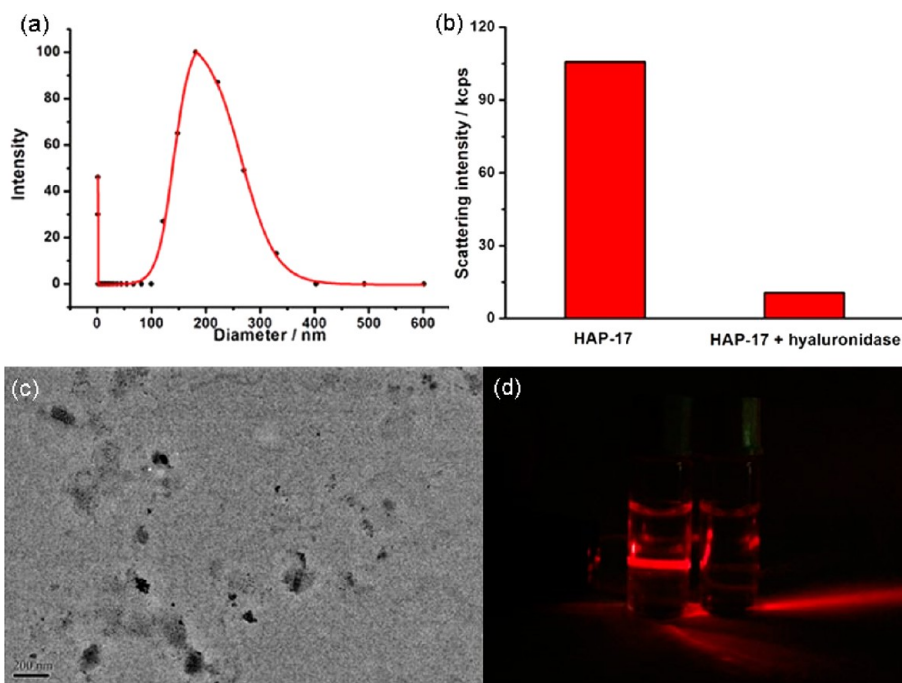


Figure 4. (a) CONTIN plots of hydrodynamic diameter and (c) TEM image of HAP-17 after hydrolyzation by hyaluronidase for 3 h. (b) Scattering-light intensity and (d) Tyndall effect of HAP-17 before (left) and after (right) hydrolyzation by hyaluronidase for 3 h.

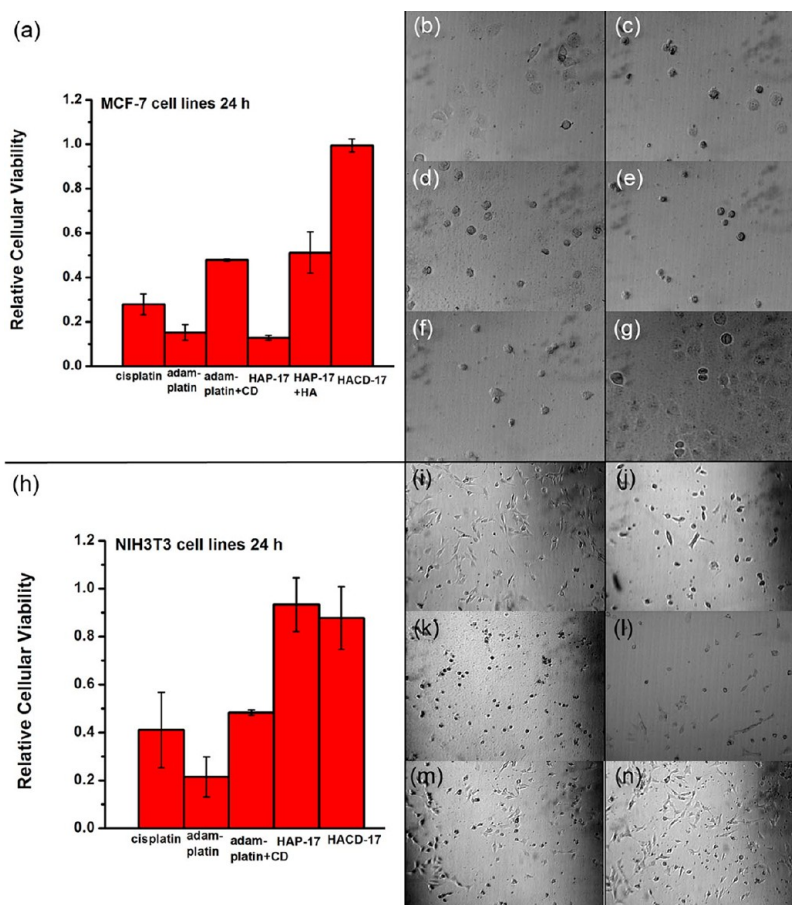


Figure 5. Relative cellular viability of (a) MCF-7 and (h) NIH3T3 cell lines after 24 h of treatment with cisplatin, adamplatin prodrug, adamplatin/ β -CD complex, HAP-17, HACD-17, and HAP-17 + excess HA. Photographs of MCF-7 cells treated with (b) blank, (c) cisplatin, (d) adamplatin prodrug, (e) HAP-17, (f) HAP-17 + excess HA, and (g) HACD-17 as well as NIH3T3 cells treated with (i) blank, (j) cisplatin, (k) adamplatin prodrug, (l) adamplatin/ β -CD complex, (m) HAP-17, and (n) HACD-17 are shown.

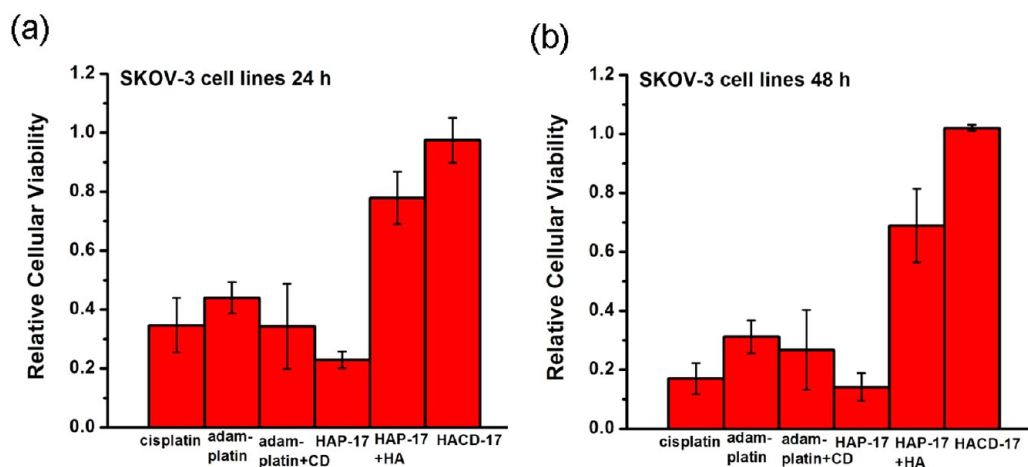


Figure 6. Relative cellular viability of SKOV-3 cell line: (a) 24 and (b) 48 h after the treatment with cisplatin, adamplatin prodrug, adamplatin/ β -CD complex, HAP-17, HACD-17, and HAP-17 with an excess of HA.

decreased by 44% when the HA receptors of MCF-7 cells were bound by an excess amount of HA polymer.

Significantly, cellular toxicity tests using the NIH3T3 cell line (mouse embryonic fibroblast cell line, HA receptor-negative^{35,61}) as a model cell line devoid of HA receptors showed that the relative cellular viability of HAP-17 stayed at 93% after 24 h, which was much higher than that of cisplatin (41%),

adamplatin prodrug (21%), and adamplatin/ β -CD complex (48%). This indicates that the HAP-17 nanoparticle is much less toxic to cells that do not express HA receptors than cisplatin, adamplatin prodrug, and adamplatin/ β -CD complex. In the control experiment, HACD-17 showed no cytotoxicity toward both the MCF-7 and NIH3T3 cell lines. In addition, the morphological changes of cancer and normal cells in the

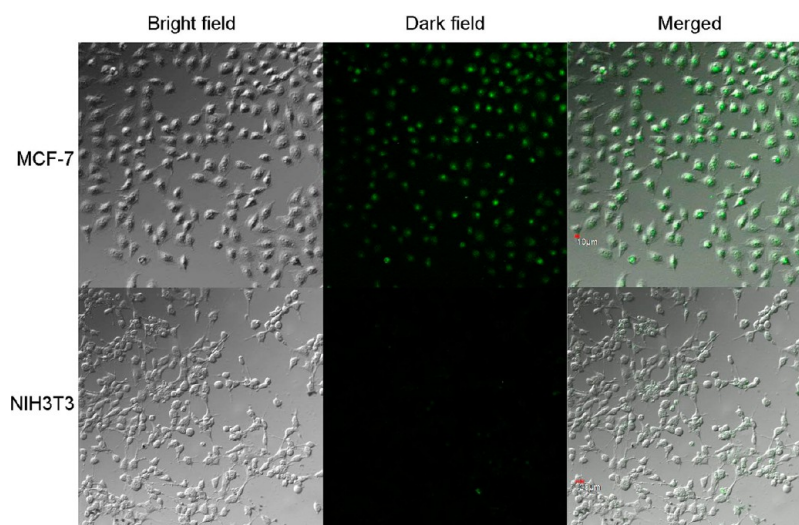


Figure 7. Bright-field (left), fluorescence (center), and merged (right) images of MCF-7 (top) and NIH3T3 cells (bottom) incubated with FITC-HAP for 6 h.

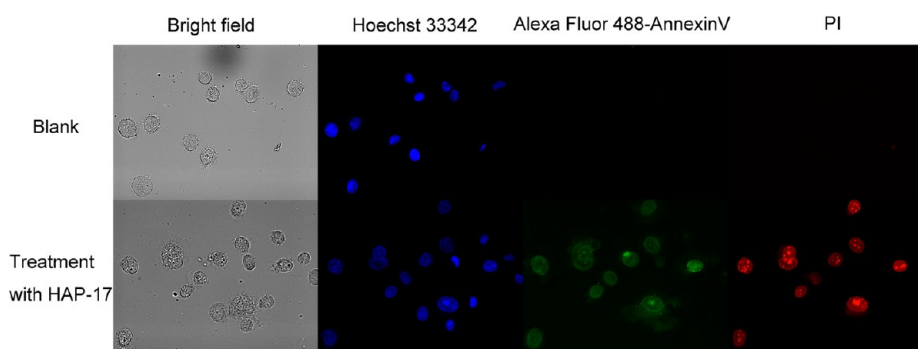


Figure 8. Apoptosis of MCF-7 cancer cells without (top) and with (bottom) the treatment with HAP-17 for 24 h. The fluorescence of Hoechst 33342, Alexa Fluor 488–AnnexinV, and PI was observed from the suspended MCF-7 cells in the dark field. The nuclei were stained by Hoechst 33342, and cells in the early and late stages of apoptosis were stained by AnnexinV and PI, respectively.

presence of cisplatin, adamplatin prodrug, HAP-17, and HACD-17 revealed that HAP-17 more effectively damaged the cancer cells than cisplatin and adamplatin prodrug (Figure 5c–e), whereas HAP-17 was less toxic toward normal cells than cisplatin and adamplatin prodrug (Figure 5j–m). This result was fully consistent with that obtained in the cell-counting experiments. Furthermore, the viability data at 48 h (see Figure S20, Supporting Information) showed much more positive results than that obtained at 24 h, verifying the conclusions mentioned earlier. Therefore, we may conclude that the HAP-17 nanoparticle is more active against cancer cells and has a much lower cytotoxicity toward normal cells than cisplatin, adamplatin prodrug, and adamplatin/ β -CD complex. A plausible explanation is that the high affinity of the HA shell of HAP-17 toward the HA receptors on cancer cells facilitates the receptor-mediated endocytosis of HAP-17 into the cancer cells, but this process is impeded in NIH3T3 cells to a great extent because of the lack of HA receptors.

Furthermore, the cytotoxicity experiments with SKOV-3 cancer cells, a human ovarian cancer cell line sensitive to cisplatin, were performed to evaluate the anticancer activities of HAP-17. As shown in Figures 6 and S21, the cellular viability of the SKOV-3 cell line (16.9%) was much lower than that of the MCF-7 cell line (29.5%) after incubation with cisplatin for 48 h. HAP-17 showed a much higher inhibition effect on the viability

of SKOV-3 cells than cisplatin, adamplatin prodrug, and adamplatin/ β -CD complex after incubation for 24 and 48 h. However, this inhibition effect dramatically decreased upon addition of HA. These results support our contention that HAP-17 selectively recognizes HA-receptor-positive cancer cells and enhances the killing ability toward cancer cells through a receptor-mediated-internalization process.

The efficient uptake of HAP into cancer cells was confirmed by fluorescent confocal images. HACD was labeled with fluorescent dye (FITC) through an amide condensation reaction to form FITC-HACD (see Figure S22, Supporting Information), and fluorescent FITC-labeled nanoparticles (FITC-HAP) were constructed by physically mixing FITC-HACD and adamplatin prodrug. After incubation with FITC-HAP for 6 h, MCF-7 cancer cells showed the bright green fluorescence of FITC, and, in sharp contrast, NIH3T3 cells exhibited only slight fluorescence, demonstrating that HAP was internalized into the cancer cells via receptor-mediated endocytosis (Figure 7).

Furthermore, we also investigated the cellular apoptosis effect of HAP-17 using the in situ counterstaining method. As shown in Figure 8, MCF-7 cancer cells were stained by Alexa Fluor 488–AnnexinV and PI after treatment with HAP-17. The morphological changes, such as cell-membrane foaming and apoptotic bodies, were clearly observed in these targeted cells,

showing that HAP-17 induced obvious apoptosis in MCF-7 cancer cells.

Tumor-Growth Inhibition Experiments in Vivo. To evaluate the antitumor effects of HAP in practical applications, tumor-growth inhibition experiments in vivo were performed using BALB/c nude mice bearing SKOV-3 cancer cells that possess strong tumorigenic ability and sensitivity toward cisplatin and its derivatives.⁶² As shown in Figure 9a, mice

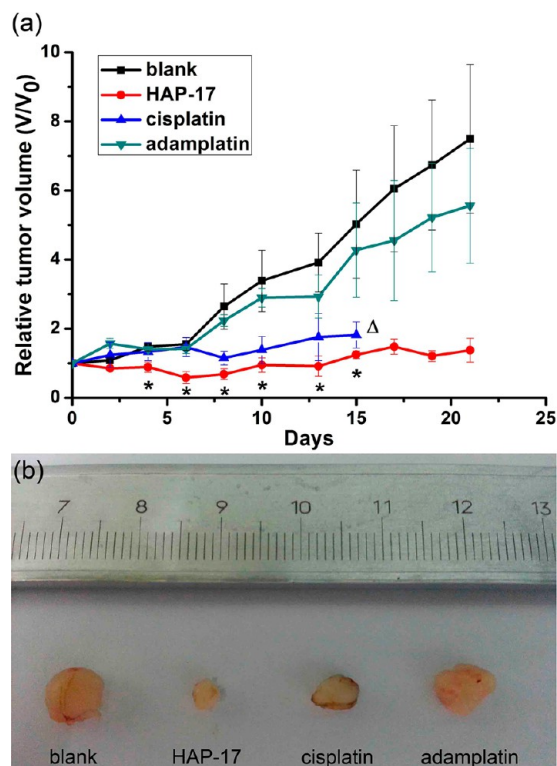


Figure 9. Tumor-growth inhibition experiments in vivo. (a) Tumor-growth curves for BALB/c nude mice bearing SKOV-3 cancer cells treated with blank control (PBS), HAP-17, cisplatin, and adamplatin prodrug. The injected dose was normalized to 3.5 mg kg⁻¹ cisplatin. The differences between cisplatin and HAP-17 that were statistically significant are indicated with asterisks ($P < 0.05$). The delta symbol indicates that mice in the cisplatin group started to die at day 15. (b) Picture of tumors in the blank control, HAP-17, cisplatin, and adamplatin prodrug groups.

with tumor were divided into four groups, one of which was untreated (blank control), and the other three groups were injected with HAP-17, cisplatin, and adamplatin prodrug by the tail vein. The tumor volumes of mice in the untreated group increased dramatically over the entire experimental period. On the basis of the aforementioned results (see Figure S17, Supporting Information), we infer that the low water solubility and poor biocompatibility significantly reduced the activity of adamplatin prodrug, ultimately resulting in the negligible antitumor efficiency for the adamplatin prodrug-treated group in vivo. In contrast, HAP-17 nanoparticles showed a better antitumor activity than the commercial anticancer drug cisplatin, giving a tumor-growth inhibition of up to 82% by day 21, which was in good agreement with the result evaluated by the weight of tumors (80%). It is noteworthy that cisplatin exhibited serious adverse effects toward mice and caused continuous body-weight loss¹⁹ and death during the entire experimental period (Figure 10). The survival rate of mice was

only 16.7% by day 25 because of the high toxicity of cisplatin toward normal cells and tissues. In contrast, the mice in the other three groups showed no appreciable body-weight loss or death. These results were consistent with the cytotoxicity experiments in vitro. A possible mechanism is the specific binding of HA on the backbone of HAP to the HA receptors overexpressed on tumor cells, which not only allows for the receptor-mediated endocytosis of HAP into tumor cells and tissues but also prevents the normal cells and tissues from damage. The anticancer activities and side effects of HAP-17, cisplatin, and adamplatin prodrug were visually distinguishable in the physical appearance of mice in terms of tumor size and body weight (Figures 9b and S23, Supporting Information).

CONCLUSIONS

In this study, we constructed a series of conjugated polysaccharides composed of hyaluronic acid (HA) main chain and cyclodextrins (CD) side chains. The HA-CD conjugates incorporating adamplatin prodrug self-assembled to form nanoparticles (HAP) possessing a hydrophilic HA backbone for recognizing cancer cells and CDs for carrying hydrophobic drugs. HAP was comprehensively tested as a delivery system for an adamplatin prodrug in vitro and in vivo. Its antitumor activity in mice was comparable to cisplatin but at much reduced toxicity. The present methodology provides a versatile HA platform for targeted drug delivery and transport into cancer cells while exhibiting minimal uptake into normal tissues.

EXPERIMENTAL SECTION

Materials Preparation. All chemicals were reagent-grade unless noted otherwise. β -CD was recrystallized twice from water and dried in vacuo at 90 °C for 24 h prior to use. Sodium hyaluronate ($M_w = 46\,000$), cisplatin, 1-ethyl-3-(3-dimethylaminopropyl)-carbodiimide (EDC), *N*-hydroxysulfosuccinimide sodium salt (NHSS), potassium tetrachloroplatinate (II) (K_2PtCl_4), fluorescein isothiocyanate isomer I (FITC), and hyaluronidase were purchased from commercial sources and used as received. Mono-6-deoxy-6-ethylenediamino- β -CD was prepared by a literature procedure.⁶³ 1-Adamantylamine was prepared by treating 1-adamantylamine hydrochloride with excess ammonia followed by filtration, washing with water, and drying in vacuo.

Instruments. NMR spectra were recorded on a Bruker AV400 instrument. For the AFM measurements, a sample solution (0.2 mg/mL) was dropped onto newly clipped mica and air-dried, and the residue obtained was examined in tapping mode in the air under ambient conditions using a Veeco Nano IIIa Multimode AFM instrument. High-resolution transmission electron microscope (HRTEM) images were obtained on a Tecnai G² F20 microscope instrument operated at 200 kV. The samples were prepared by placing a drop of solution (0.2 mg/mL) on a carbon-coated copper grid. The samples for SEM measurements were prepared by dropping each sample solution onto a coverslip followed by evaporation of the solvent at room temperature. SEM experiments were performed on a Shimadzu SS-550 scanning electron microscope. The sample solutions for DLS experiments were prepared by filtering each solution through a 450 nm syringe-driven filter (JET BIOFIL) into a clean scintillation vial. The samples were examined on a Brookhaven BI-200SM laser light scattering spectrometer equipped with a digital correlator (BI-9000AT) at $\lambda = 636$ nm at 25 °C. All DLS measurements were performed at the scattering angle of 90°. The zeta potential was recorded on a Brookhaven ZETAPALS/BI-200SM at 25.5 °C. GPC measurements were employed to examine the weight-averaged molecular weights (M_w) of polymers on a four detection size-exclusion chromatograph (Four-SEC) containing a Waters 1525 separation module connected with a Viscotek M302 four detector array, a combination of refractive index, light scattering (LS angle, 7 and 90°;

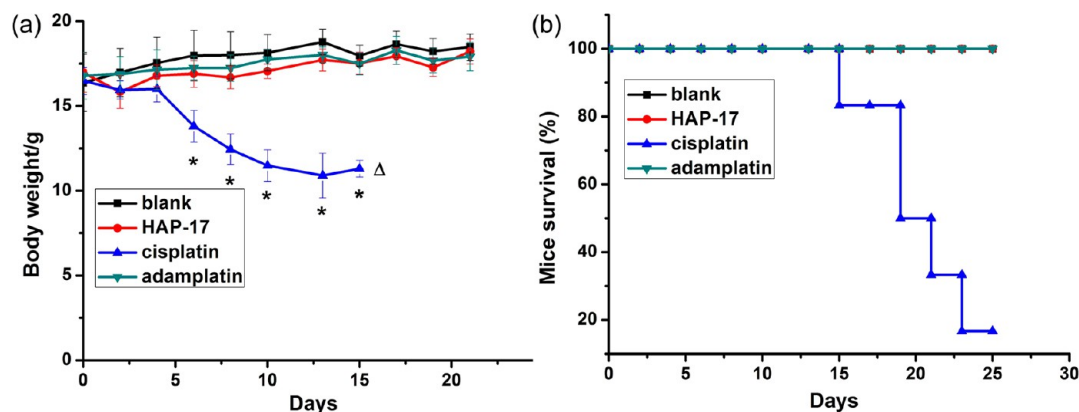


Figure 10. (a) Body-weight curves for BALB/c nude mice bearing SKOV-3 cancer cells after treatment with blank control (PBS), HAP-17, cisplatin, and adamplatin prodrug. The differences between cisplatin and HAP-17 that were statistically significant are indicated with asterisks ($P < 0.01$). The delta symbol indicates that mice in the cisplatin group started to die at day 15. (b) Survival curves of BALB/c nude mice bearing SKOV-3 cancer cells after treatment with HAP-17, cisplatin, adamplatin, and blank control (PBS).

laser wavelength, $\lambda = 532$ nm), viscosity detector, and UV-vis detector. Two mixed-bed SEC columns (GMH_{HR}-M and GMH_{HR}-H from Viscotek) were used. Poly(ethylene oxide) was used as the calibration standard, and 0.1 M phosphate buffer (pH = 7.2) was used as the mobile phase at a flow rate of 1.0 mL min⁻¹ at an operating temperature of 25 °C. The fluorescent confocal images were carried out on an Olympus FV1000S-IX81 fluorescence microscope ($\lambda_{\text{ex}} = 405$ nm, 25 °C).

Preparation of β -CD-Modified Hyaluronate Acid (HACD). 1-Ethyl-3-(3-dimethyl aminopropyl)carbodiimide (EDC) (167.7 mg, 0.875 mmol) and *N*-hydroxysulfosuccinimide sodium salt (NHSS) (190 mg, 0.875 mmol) were added to a solution of sodium hyaluronate ($M_w = 46000$) (100 mg, 2.17 μ mol) in phosphate buffer solution (PBS, 0.1 M, pH 7.2) (30 mL), and the mixture was stirred at 25 °C for 30 min. Then, various amounts of mono-6-deoxy-6-ethylenediamino- β -CD (73.6–588.5 mg, 0.0625–0.5 mmol) in PBS (10 mL) was added, and the mixture was stirred for 24 h at room temperature. The resulting solution was dialyzed against an excess amount of deionized water for 5 days. After being freeze-dried, HACDs with different degrees of substitution were obtained as white powder. ¹H NMR (400 MHz, D₂O, ppm): (1) HACD-5.6: δ 1.95 (s, 3H, H of methyl group of HA), 3.02–3.91 (m, 12.04H, H of HA and C-3, C-5, C-6, C-2, C-4, and methylene on ethanediamine group of β -CD), 4.44–4.48 (m, 2H, H of HA), 5.02–5.08 (m, 0.34H, H of C-1 of β -CD); (2) HACD-11.5: δ 1.98 (s, 3H, H of methyl group of HA), 3.05–4.14 (m, 14.19H, H of HA and C-3, C-5, C-6, C-2, C-4, and methylene on ethanediamine group of β -CD), 4.47–4.51 (m, 2H, H of HA), 5.05–5.11 (m, 0.7H, H of C-1 of β -CD); (3) HACD-16: δ 1.95 (s, 3H, H of methyl group of HA), 3.04–3.94 (m, 16.23H, H of HA and C-3, C-5, C-6, C-2, C-4, and methylene on ethanediamine group of β -CD), 4.43–4.48 (m, 2H, H of HA), 5.02–5.08 (m, 0.99H, H of C-1 of β -CD); (4) HACD-17: δ 1.97 (s, 3H, H of methyl group of HA), 3.06–3.93 (m, 16.24H, H of HA and C-3, C-5, C-6, C-2, C-4, and methylene on ethanediamine group of β -CD), 4.45–4.50 (m, 2H, H of HA), 5.04–5.10 (m, 1.06H, H of C-1 of β -CD).

Preparation of FITC/ β -CD-Modified Hyaluronate Acid (FITC-HACD). Amino-functionalized FITC was prepared according to reported procedures.⁶⁴ 1-Ethyl-3-(3-dimethyl aminopropyl)carbodiimide (EDC) (83.8 mg, 0.44 mmol) and *N*-hydroxysulfosuccinimide sodium salt (NHSS) (95 mg, 0.44 mmol) were added to a solution of sodium hyaluronate ($M_w = 46000$) (50 mg, 1.08 μ mol) in PBS (0.1 M, pH 7.2) (30 mL), and the mixture was stirred for 30 min at 25 °C. Then, mono-6-deoxy-6-ethylenediamino- β -CD (294.2 mg, 0.25 mmol) and amino-functionalized FITC (112.4 mg, 0.25 mmol) in PBS (10 mL) were added, and the mixture was stirred at room temperature for 24 h. The resulting solution was dialyzed against an excess amount of deionized water for 7 days. After being freeze-dried, FITC-HACD was obtained as pale-yellow powder. The content of FITC molecules in the conjugate was calculated as 0.22 wt %, which

was determined using a UV-vis calibration curve of amino-functionalized FITC at $\lambda = 485$ nm.

Preparation of Adamplatin Prodrug. Adamplatin prodrug was prepared by literature procedures with slight modification.⁵³ In brief, K₂PtCl₄ (210 mg, 0.51 mmol) dissolved in distilled water (5 mL) was added to a solution of KI (672 mg, 4.05 mmol) in distilled water (2 mL). The mixture stood for 15 min to obtain a dark brown aqueous solution of K₂PtI₄. 1-Adamantylamine (152 mg, 1 mmol) was suspended in distilled water (5 mL) and added to the above-mentioned solution to immediately form a yellow precipitate. The mixture was stirred overnight at 30 °C and filtered, and the yellow precipitate was washed with distilled water until no halide ion was detected. The obtained yellow solid was suspended in a mixed solvent composed of water and acetone (1:1, 60 mL) again, and AgNO₃ (157.1 mg, 0.92 mmol) was added. The mixture was stirred for 48 h at 25 °C in the dark. The resulting mixture was filtered, and KCl (69.0 mg, 0.92 mmol) was added to the filtrate. The pale-yellow precipitate appeared immediately after the removal of acetone under reduced pressure and was filtered, washed repeatedly with distilled water, and dried. The adamplatin prodrug was obtained as a pale-yellow solid (63% yield). ¹H NMR (400 MHz, DMSO-*d*₆, TMS): δ 1.58–1.62 (m, 6H, H of adamantane), 1.90–2.08 (m, 9H, H of adamantane), 4.43 (brs, 1H, part of H of -NH₂). ESI-MS *m/z*: 533.1 [M - Cl]⁺, 496.3 [M - 2Cl - H]⁺.

Preparation of HACD-Adamplatin Nanoparticles (HAPs). Adamplatin prodrug (0.19 mg, 0.34 μ mol) in DMSO (30 μ L) was added to a solution of HACD-17 (1.27 mg, 0.02 μ mol, containing 0.34 μ mol β -CD) in deionized water/PBS (1 mL), and then the mixture was ultrasonicated for 10 min. The resulting HAP-17 solution ([Pt] = 0.34 mM) was stored at 4 °C. Other HAPs with different Ds by β -CD were prepared by similar procedures.

Loading Level of Adamplatin in HAP-17. HACD-17 (4.8 mg, 0.076 μ mol, containing 1.28 μ mol β -CD) was dissolved in deionized water (2.5 mL), and then various amounts of adamplatin (0.081–2.92 mg, 0.14–5.14 μ mol) in 75 μ L of DMSO were added to the solution prepared above. Any insoluble substance was removed through a syringe filter (450 nm), the filtrate was dialyzed against an excess amount of deionized water for 1 h, and the volume of the resulting solution was standardized to 5 mL. The concentration of platinum in the solution was determined using atomic emission spectrometry.

Enzyme-Triggered Drug-Release Experiments. Adamplatin prodrug (0.17 mg, 0.30 μ mol) in DMSO (30 μ L) was added to a solution of HACD-17 (1.13 mg, 0.018 μ mol, containing 0.30 μ mol β -CD) in deionized water (10 mL), and then the mixture was ultrasonicated for 10 min. After that, hyaluronidase was added (the final concentration of hyaluronidase was 0.5 IU mL⁻¹), and the solution was stirred for 3 h at 37 °C. The obtained solution was subjected to examination by DLS, TEM, and Tyndall effect.

Cytotoxicity Experiments. MCF-7 human breast cancer cells, NIH3T3 mouse embryonic fibroblasts, and SKOV-3 human ovarian cancer cells were cultured in Dulbecco's modified Eagle's medium (DMEM), which was supplemented with 10% fetal bovine serum (FBS), in 24-well plates (2×10^4 cells mL⁻¹, 1 mL per well) for 24 h. The cells were incubated with cisplatin, adamplatin, HAP-17, HAP-17 + excess HA, and HACD-17 ([Pt] = 17 μ M, [HACD] = 1 μ M). After incubation for 24 and 48 h, the relative cellular viability was measured using a cell-counting assay.

Furthermore, MTT assays were performed to evaluate the IC₅₀ values of adamplatin and HAP-17 toward the MCF-7 cell line. Briefly, MCF-7 human breast cancer cells were cultured for 24 h in DMEM supplemented with 10% FBS in 96-well plates (1000 cells in 100 μ L of medium per well). The cells were incubated with adamplatin and HAP-17 at different concentrations for another 24 h. The cell inhibitory rates were determined by the MTT assay. All data are presented as the mean \pm standard deviation.

Fluorescent Confocal Imaging. MCF-7 human breast cancer cells and NIH3T3 mouse embryonic fibroblasts were cultured for 24 h in DMEM supplemented with 10% fetal bovine serum (FBS) in 6-well plates (2×10^4 cells mL⁻¹, 2 mL per well). The cells were incubated with FITC-HAP ([adamplatin prodrug] = 17 μ M, [FITC-HACD] = 1 μ M). After incubation for 6 h, the culture medium was removed, and the cells were washed with PBS and subjected to observation by a fluorescence microscope.

Apoptosis Experiments. MCF-7 human breast cancer cells were cultured in DMEM supplemented with 10% fetal bovine serum (FBS) in 6-well plates (5×10^4 cells mL⁻¹, 2 mL per well) for 24 h. The cells were incubated with HAP-17 ([adamplatin prodrug] = 17 μ M, [HACD-17] = 1 μ M) for 24 h, and they were then washed with cold PBS. The cells were detached with trypsin and then resuspended in PBS. After centrifugation (800 rpm) for 3 min, the supernatant was discarded, and the cells were resuspended in 1 \times annexin buffer (100 μ L) and treated with Alexa Fluor 488–Annexin V (15 μ L), PI solution (2 μ L), 600 \times Hoechst 33342 solution (20 μ L), and 1 \times annexin buffer (80 μ L). The suspension was incubated at room temperature for 15 min and then centrifuged (400 rpm) for 5 min. The supernatant was discarded, and the cells were resuspended in 1 \times annexin buffer (100 μ L). The cells were observed using a fluorescence microscope.

Animal Model Experiment. All experimental procedures were approved and in accordance with China's National Code of Animal Care for Scientific Experimentation. The experiment was also assessed by the Animal Experimentation Ethics Committee of Nankai University. Four-week-old female BALB/c nude mice ($n = 24$) received 5×10^6 SKOV-3 cells in DMEM (100 μ L) into the left groin by subcutaneous injection. When the tumor volume reached 50–100 mm³ (ca. 14 days after tumor implantation), the mice were divided into four groups (six mice per group). The groups were injected with 200 μ L of either PBS, HAP-17, cisplatin, and adamplatin prodrug every 3 days through the tail vein. The doses were set at 3.5 mg kg⁻¹ cisplatin. The tumor volumes (V) were measured using a caliper every 2 days and calculated using the following equation: $V = 0.5 \times (\text{tumor length}) \times (\text{tumor width})^2$. The relative tumor volumes were calculated as V/V_0 (V_0 is the tumor volume when drug injection began).

Statistical analysis of the data was carried out using the Student's t test. Differences were considered statistically significant if the P value was <0.05 .

■ ASSOCIATED CONTENT

● Supporting Information

Characterization of HACDs, adamplatin prodrug, and HAPs; Job's plot of adamplatin prodrug and β -CD; IC₅₀ of HAP-17 and adamplatin prodrug; cytotoxicity after drug treatment for 48 h; synthetic route for FITC-HACD; and side-effect images of drug-treated cancer-bearing nude mice. This material is available free of charge via the Internet at <http://pubs.acs.org>.

■ AUTHOR INFORMATION

Corresponding Author

*E-mail: yuliu@nankai.edu.cn. Phone: +86-22-23503625.

Notes

The authors declare no competing financial interest.

■ ACKNOWLEDGMENTS

We thank the 973 Program (2011CB932502) and NNSFC (20932004, 91027007, 91227107, and 21102075) for financial support.

■ ABBREVIATIONS USED

HA, hyaluronic acid; HACD, β -cyclodextrin modified hyaluronic acid; HAP, hyaluronic acid particles

■ REFERENCES

- (1) Calderera-Moore, M. E.; Liechty, W. B.; Peppas, N. Responsive theranostic systems: Integration of diagnostic imaging agents and responsive controlled release drug delivery carriers. *Acc. Chem. Res.* **2011**, *44*, 1061–1070.
- (2) Mintzer, M. A.; Simanek, E. E. Nonviral vectors for gene delivery. *Chem. Rev.* **2009**, *109*, 259–302.
- (3) Lee, S.; Chen, H.; O'Halloran, T. V.; Nguyen, S. T. Clickable polymer-caged nanobins as a modular drug delivery platform. *J. Am. Chem. Soc.* **2009**, *131*, 9311–9320.
- (4) Al-Jamal, W. T.; Kostarelos, K. Liposomes: From a clinically established drug delivery system to a nanoparticle platform for theranostic nanomedicine. *Acc. Chem. Res.* **2011**, *44*, 1094–1104.
- (5) Landmark, K. J.; DiMaggio, S.; Ward, J.; Kelly, C.; Vogt, S.; Hong, S.; Kotlyar, A.; Myc, A.; Thomas, T. P.; Penner-Hahn, J. E.; Baker, J. R., Jr.; Holl, M. M. B.; Orr, B. J. Synthesis, characterization, and in vitro testing of superparamagnetic iron oxide nanoparticles targeted using folic acid-conjugated dendrimers. *ACS Nano* **2008**, *2*, 773–783.
- (6) Hayashi, K.; Ono, K.; Suzuki, H.; Sawada, M.; Moriya, M.; Sakamoto, W.; Yogo, T. High-frequency, magnetic-field-responsive drug release from magnetic nanoparticle/organic hybrid based on hyperthermic effect. *ACS Appl. Mater. Interfaces* **2010**, *2*, 1903–1911.
- (7) Ambrogio, M. W.; Thomas, C. R.; Zhao, Y.; Zink, J. I.; Stoddart, J. F. Mechanized silica nanoparticles: A new frontier in theranostic nanomedicine. *Acc. Chem. Res.* **2011**, *44*, 903–913.
- (8) Vallet-Regi, M.; Colilla, M.; Gonzalez, B. Medical applications of organic-inorganic hybrid materials within the field of silica-based bioceramics. *Chem. Soc. Rev.* **2011**, *40*, 596–607.
- (9) Du, J.; Sun, T.; Song, W.; Wu, J.; Wang, J. A tumor-acidity-activated charge-conversional nanogel as an intelligent vehicle for promoted tumoral-cell uptake and drug delivery. *Angew. Chem., Int. Ed.* **2010**, *49*, 3621–3626.
- (10) Soppimath, K. S.; Liu, L.-H.; Seow, W. Y.; Liu, S.-Q.; Powell, R.; Chan, P.; Yang, Y. Multifunctional core/shell nanoparticles self-assembled from pH-induced thermosensitive polymers for targeted intracellular anticancer drug delivery. *Adv. Funct. Mater.* **2007**, *17*, 355–362.
- (11) Dam, H. H.; Caruso, F. Construction and degradation of polyrotaxane multilayers. *Adv. Mater.* **2011**, *23*, 3026–3029.
- (12) Tanner, P.; Baumann, P.; Enea, R.; Onaca, O.; Palivan, C.; Meier, W. Polymeric vesicles: From drug carriers to nanoreactors and artificial organelles. *Acc. Chem. Res.* **2011**, *44*, 1039–1049.
- (13) Kim, E.; Kim, D.; Jung, H.; Lee, J.; Paul, S.; Selvapalam, N.; Yang, Y.; Lim, N.; Park, C. G.; Kim, K. Facile, template-free synthesis of stimuli-responsive polymer nanocapsules for targeted drug delivery. *Angew. Chem., Int. Ed.* **2010**, *49*, 4405–4408.
- (14) Liu, Z.; Sun, X.; Nakayama-Ratchford, N.; Dai, H. Supramolecular chemistry on water-soluble carbon nanotubes for drug loading and delivery. *ACS Nano* **2007**, *1*, 50–56.

- (15) Liu, Z.; Robinson, J. T.; Sun, X.; Dai, H. PEGylated nanographene oxide for delivery of water-insoluble cancer drugs. *J. Am. Chem. Soc.* **2008**, *130*, 10876–10877.
- (16) Dhar, S.; Liu, Z.; Thomale, J.; Dai, H.; Lippard, S. J. Targeted single-wall carbon nanotube-mediated Pt(IV) prodrug delivery using folate as a homing device. *J. Am. Chem. Soc.* **2008**, *130*, 11467–11476.
- (17) Sun, X.; Liu, Z.; Welsher, K.; Robinson, J. T.; Goodwin, A.; Zaric, S.; Dai, H. Nano-graphene oxide for cellular imaging and drug delivery. *Nano Res.* **2008**, *1*, 203–212.
- (18) Zhang, L.; Xia, J.; Zhao, Q.; Liu, L.; Zhang, Z. Functional graphene oxide as a nanocarrier for controlled loading and targeted delivery of mixed anticancer drugs. *Small* **2010**, *6*, 537–544.
- (19) Yang, Y.; Zhang, Y.-M.; Chen, Y.; Zhao, D.; Chen, J.-T.; Liu, Y. Construction of a graphene oxide based noncovalent multiple nanosupramolecular assembly as a scaffold for drug delivery. *Chem.—Eur. J.* **2012**, *18*, 4208–4215.
- (20) Liu, Z.; Tabakman, S.; Welsher, K.; Dai, H. Carbon nanotubes in biology and medicine: In vitro and in vivo detection, imaging and drug delivery. *Nano Res.* **2009**, *2*, 85–120.
- (21) Ghaderi, S.; Ramesh, B.; Seifalian, A. M. Fluorescence nanoparticles “quantum dots” as drug delivery system and their toxicity. *J. Drug Targeting* **2011**, *19*, 475–486.
- (22) Kreuter, J. Evaluation of nanoparticles as drug-delivery systems, III: Materials, stability, toxicity, possibilities of targeting, and use. *Pharm. Acta Helv.* **1983**, *58*, 242–250.
- (23) Mizrahy, S.; Peer, D. Polysaccharide as building blocks for nanotherapeutics. *Chem. Soc. Rev.* **2012**, *41*, 2623–2640.
- (24) Sung, H.-W.; Sonaje, K.; Liao, Z.-X.; Hsu, L.-W.; Chuang, E.-Y. pH-Responsive nanoparticles shelled with chitosan for oral delivery of insulin: From mechanism to therapeutic applications. *Acc. Chem. Res.* **2012**, *45*, 619–629.
- (25) Seeberger, P. H.; Werz, D. B. Synthesis and medical applications of oligosaccharides. *Nature* **2007**, *446*, 1046–1051.
- (26) Langer, R. New methods of drug delivery. *Science* **1990**, *249*, 1527–1533.
- (27) Seliktar, D. Designing cell-compatible hydrogels for biomedical applications. *Science* **2012**, *336*, 1124–1128.
- (28) Peer, D.; Margalit, R. Loading mitomycin C inside long circulating hyaluronan targeted nano-liposomes increases its antitumor activity in three mice tumor models. *Int. J. Cancer* **2004**, *108*, 780–789.
- (29) Rivkin, I.; Cohen, K.; Koffler, J.; Melikhov, D.; Peer, D.; Margalit, R. Paclitaxel-clusters coated with hyaluronan as selective tumor-targeted nanovectors. *Biomaterials* **2010**, *31*, 7106–7114.
- (30) Bachar, G.; Cohen, K.; Hod, R.; Feinmesser, R.; Mizrahi, A.; Shpitzer, T.; Katz, O.; Peer, D. Hyaluronan-grafted particle clusters loaded with mitomycin C as selective nanovectors for primary head and neck cancers. *Biomaterials* **2011**, *32*, 4840–4848.
- (31) Park, K. M.; Yang, J.-A.; Jung, H.; Yeom, J.; Park, J. S.; Park, K.-H.; Hoffman, A. S.; Hahn, S. K.; Kim, K. In situ supramolecular assembly and modular modification of hyaluronic acid hydrogels for 3D cellular engineering. *ACS Nano* **2012**, *6*, 2960–2968.
- (32) Han, S.-Y.; Han, H. S.; Lee, S. C.; Kang, Y. M.; Kim, I.-S.; Park, J. H. Mineralized hyaluronic acid nanoparticles as a robust drug carrier. *J. Mater. Chem.* **2011**, *21*, 7996–8001.
- (33) Luo, Y.; Prestwich, G. D. Synthesis and selective cytotoxicity of a hyaluronic acid-antitumor bioconjugate. *Bioconjugate Chem.* **1999**, *10*, 755–763.
- (34) Luo, Y.; Ziebell, M. R.; Prestwich, G. D. A hyaluronic acid-taxol antitumor bioconjugate targeted to cancer cells. *Biomacromolecules* **2000**, *1*, 208–218.
- (35) Lee, H.; Lee, K.; Park, T. G. Hyaluronic acid-paclitaxel conjugate micelles: Synthesis, characterization, and antitumor activity. *Bioconjugate Chem.* **2008**, *19*, 1319–1325.
- (36) Lee, M.-Y.; Park, S.-J.; Park, K.; Kim, K. S.; Lee, H.; Hahn, S. K. Target-specific gene silencing of layer-by-layer assembled gold-cysteamine/siRNA/PEI/HA nanocomplex. *ACS Nano* **2011**, *5*, 6138–6147.
- (37) Choi, K. Y.; Min, K. H.; Na, J. H.; Choi, K.; Kim, K.; Park, J. H.; Kwon, I. C.; Jeong, S. Y. Self-assembled hyaluronic acid nanoparticles as a potential drug carrier for cancer therapy: Synthesis, characterization, and in vivo biodistribution. *J. Mater. Chem.* **2009**, *19*, 4102–4107.
- (38) Choi, K. Y.; Chung, H.; Min, K. H.; Yoon, H. Y.; Kim, K.; Park, J. H.; Kwon, I. C.; Jeong, S. Y. Self-assembled hyaluronic acid nanoparticles for active tumor targeting. *Biomaterials* **2010**, *31*, 106–114.
- (39) Choi, K. Y.; Min, K. H.; Yoon, H. Y.; Kim, K.; Park, J. H.; Kwon, I. C.; Choi, K.; Jeong, S. Y. PEGylation of hyaluronic acid nanoparticles improves tumor targetability in vivo. *Biomaterials* **2011**, *32*, 1880–1889.
- (40) Choi, K. Y.; Yoon, H. Y.; Kim, J.-H.; Bae, S. M.; Park, R.-W.; Kang, Y. M.; Kim, I.-S.; Kwon, I. C.; Choi, K.; Jeong, S. Y.; Kim, K.; Park, J. H. Smart nanocarrier based on PEGylated hyaluronic acid for cancer therapy. *ACS Nano* **2011**, *5*, 8591–8599.
- (41) Peer, D.; Park, E. J.; Morishita, Y.; Carman, C. V.; Shimaoka, M. Systemic leukocyte-directed siRNA delivery revealing cyclin D1 as an anti-inflammatory target. *Science* **2008**, *319*, 627–630.
- (42) Peer, D.; Zhu, P.; Carman, C. V.; Lieberman, J.; Shimaoka, M. Selective gene silencing in activated leukocytes by targeting siRNAs to the integrin lymphocyte function-associated antigen-1. *Proc. Natl. Acad. Sci. U.S.A.* **2007**, *104*, 4095–4100.
- (43) Liu, G.; Choi, K. Y.; Bhirde, A.; Swierczewska, M.; Yin, J.; Lee, S. W.; Park, J. H.; Hong, J. I.; Xie, J.; Niu, G.; Kiesewetter, D. O.; Lee, S.; Chen, X. Sticky nanoparticles: A platform for siRNA delivery by a bis(zinc(II) dipicolylamine)-functionalized, self-assembled nanoconjugate. *Angew. Chem., Int. Ed.* **2012**, *51*, 445–449.
- (44) Chen, Y.; Liu, Y. Cyclodextrin-based bioactive supramolecular assemblies. *Chem. Soc. Rev.* **2010**, *39*, 495–505.
- (45) Chen, Y.; Zhang, Y.-M.; Liu, Y. Multidimensional nano-architectures based on cyclodextrins. *Chem. Commun.* **2010**, *46*, S622–S633.
- (46) Yokoyama, M.; Okano, T.; Sakurai, Y.; Suwa, S.; Kataoka, K. Introduction of cisplatin into polymeric micelle. *J. Controlled Release* **1996**, *39*, 351–356.
- (47) Eftink, M. R.; Andy, M. L.; Bystrom, K.; Perlmutter, H. D.; Kristol, D. S. Cyclodextrin inclusion complexes: Studies of the variation in the size of alicyclic guests. *J. Am. Chem. Soc.* **1989**, *111*, 6765–6772.
- (48) Toole, B. P. Hyaluronan: From extracellular glue to pericellular cue. *Nat. Rev. Cancer* **2004**, *4*, 528–539.
- (49) Bertrand, P.; Girard, N.; Duval, C.; d’Anjou, J.; Chauzy, C.; Menard, J.-F.; Delpech, B. Increased hyaluronidase levels in breast tumor metastases. *Int. J. Cancer* **1997**, *73*, 327–331.
- (50) Lokeshwar, V. B.; Lokeshwar, B. L.; Pham, H. T.; Block, N. L. Association of elevated levels of hyaluronidase, a matrix-degrading enzyme, with prostate cancer progression. *Cancer Res.* **1996**, *56*, 651–657.
- (51) Stern, R. Hyaluronidase in cancer biology. *Semin. Cancer Biol.* **2008**, *18*, 275–280.
- (52) Jaracz, S.; Chen, J.; Kuznetsova, L. V.; Ojima, I. Recent advances in tumor-targeting anticancer drug conjugates. *Bioorg. Med. Chem.* **2005**, *13*, 5043–5054.
- (53) Tang, W.; Qu, Y.; Tai, A.; Ji, X.; Zhang, F.; Liu, L. Synthesis characterization of Pt^{II} Pt^{IV} complexes of amantadine and their antitumor activity against L-1210 in BDF/2. *Nanjing Daxue Xuebao, Ziran Kexue* **1984**, *471*–478.
- (54) Kasparkova, J.; Novakova, O.; Vrana, O.; Intini, F.; Natile, G.; Brabec, V. Molecular aspects of antitumor effects of a new platinum (VI) drug. *Mol. Pharmacol.* **2006**, *70*, 1708–1719.
- (55) Woollins, J. D.; Woollins, A.; Rosenberg, B. The detection of trace amounts trans-Pt(NH₃)₂Cl₂ in the presence of cis-Pt(NH₃)₂Cl₂. A high performance liquid chromatographic application of kurnakow’s test. *Polyhedron* **1983**, *2*, 175–178.
- (56) Zhang, Y.-M.; Chen, Y.; Li, Z.-Q.; Li, N.; Liu, Y. Quinolinotriazole-β-cyclodextrin and its adamantanecarboxylic acid complex as efficient water-soluble fluorescent Cd²⁺ sensors. *Bioorg. Med. Chem.* **2010**, *18*, 1415–1420.

(57) Nitta, K.; Miyake, J.; Watanabe, J.; Ikeda, Y. Gel formation driven by tunable hydrophobic domain: Design of acrylamide macromonomer with oligo hydrophobic segment. *Biomacromolecules* **2012**, *13*, 1002–1009.

(58) Needham, C. J.; Williams, A. K.; Chew, S. A.; Kasper, F. K.; Mikos, A. G. Engineering a polymeric gene delivery vector based on poly(ethylenimine) and hyaluronic acid. *Biomacromolecules* **2012**, *13*, 1429–1437.

(59) Lee, H.; Mok, H.; Lee, S.; Oh, Y. K.; Park, T. G. Target-specific intracellular delivery of siRNA using degradable hyaluronic acid nanogels. *J. Controlled Release* **2007**, *119*, 245–252.

(60) Caron, G.; Ermondi, G.; Gariboldi, M. B.; Monti, E.; Gabano, E.; Ravera, M.; Osella, D. The relevance of polar surface area (PSA) in rationalizing biological properties of several *cis*-diamminemalonatoplatinum (II) derivatives. *ChemMedChem* **2009**, *4*, 1677–1685.

(61) Luo, Y.; Bernshaw, N. J.; Lu, Z.; Lopecek, J.; Prestwich, G. D. Targeted delivery of doxorubicin by HPMA copolymer-hyaluronan bioconjugates. *Pharm. Res.* **2002**, *19*, 396–402.

(62) Xiao, H.; Song, H.; Zhang, Y.; Qi, R.; Wang, R.; Xie, Z.; Huang, Y.; Li, Y.; Wu, Y.; Jing, X. The use of polymeric platinum(IV) prodrugs to deliver multinuclear platinum(II) drugs with reduced systemic toxicity and enhanced antitumor efficacy. *Biomaterials* **2012**, *33*, 8657–8669.

(63) May, B. L.; Kean, S. D.; Easton, C. J.; Lincoln, S. F. Preparation and characterization of 6^A-polyamine-mono-substituted β -cyclodextrins. *J. Chem. Soc., Perkin Trans. 1* **1997**, 3157–3160.

(64) Gentsch, R.; Pippig, F.; Nilles, K.; Theato, P.; Kikkeri, R.; Maglinao, M.; Lepenies, B.; Seeberger, P. H.; Borner, H. G. Modular approach toward bioactive fiber meshes carrying oligosaccharides. *Macromolecules* **2010**, *43*, 9239–9247.